Tuning the Viscosity Profiles of High- T g Poly(1,2,3-triazolium) Covalent Adaptable Networks by the Chemical Structure of the N-Substituents

Hatem Ben Romdhane, Omaima Anaya, Antoine Jourdain, Iurii Antoniuk, Hatem Ben Romdhane, Damien Montarnal, Eric Drockenmuller

Tuning the viscosity profiles of high Tg poly(1,2,3-triazolium) covalent adaptable networks by the chemical structure of the N-substituents

Omaima Anaya,[a,b] Antoine Jourdain,[a] Iurii Antoniuk,[a] Hatem Ben Romdhane,[b] Damien Montarnal,[c] and Eric Drockenmuller,*[a]*

[a] Univ Lyon, Université Lyon 1, CNRS, Ingénierie des Matériaux Polymères, UMR 5223, F-69003 Lyon, France.

[b] Université de Tunis El Manar, Faculté des Sciences de Tunis, Laboratoire de Chimie (Bio)Organique Structurale et de Polymères − Synthèse et Etudes Physicochimiques (LR99ES14), 2092 El Manar, Tunisia.

[c] Univ Lyon, CPE Lyon, CNRS, Catalyse, Chimie, Polymères et Procédés, UMR 5265, F-69003, Lyon, France.

TOC abstract: Correlation between chemical composition and temperature-dependent rheological properties in a series of poly(1,2,3-triazolium)-based covalent adaptable networks shows that relaxation dynamics are mostly dependent on the chemical structure of the *N*-substituents.
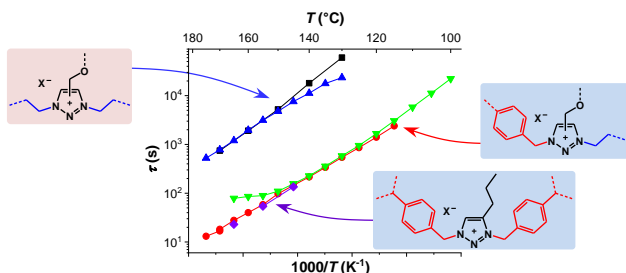
ABSTRACT. A designed library of covalent adaptable networks (CANs) having 1,2,3-triazolium dynamic cross-links are obtained through the combination of solvent- and catalyst-free thermally induced azide-alkyne cycloaddition and *N*-alkylation reactions. The use of rigid heterocyclic or aromatic segments affords CANs with greatly extended range of thermomechanical profiles, with T_gs up to 146 °C, dramatic changes in relaxation times (from 1.5 h to less than 2 min at 150 °C) depending on the chemical structure of the *N*-substituents of 1,2,3-triazolium cross-links, and tunable rubbery plateaus, with nearly constant elastic moduli up to ca. 160 °C. A detailed correlation between the rheological properties and the chemical compositions of these CANs shows that the relaxation dynamics of the networks are mainly determined by the chemical structure of the *N*-substituents of the 1,2,3-triazolium cross-links, and are independent both from the composition of the surrounding polymer networks and the corresponding T_g, at temperatures ranging from T_g + 20 °C to ca. 180 °C.

INTRODUCTION

Thermosetting polymers made of permanently cross-linked three-dimensional networks are essential in a broad variety of applications requiring high creep and solvent resistance, at ambient temperatures such as elastomers, or at high temperatures such as composite materials for coatings, adhesives, sealants, consumer goods, wind-energy, automotive, aeronautics or aerospace applications.[1] However, their inability to be recycled or reprocessed results in considerable production wastes and, together with difficulties in sorting mixed plastics sources, represents a serious bottleneck for the future circular economy of plastics. Meanwhile, public and private stakeholders multiply directives and ambitions to reach desired recycling and reusing of thermosetting materials.[2] Classical alternatives to thermosets aim at controlling the temperature dependence of the viscosity profiles of functionalized thermoplastics by strongly increasing their viscosity at low temperatures while marginally affecting their processability at higher temperatures. All strategies developed over the years rely on the formation of a transient network that maintains a mechanical continuity through the material, but these strategies differ by the length scales associated with this network. Thermoplastic elastomers rely on the formation of semi-crystalline or glassy polymer phases at the 5-100 nm range,[3] while supramolecular networks relying on hydrogen bonding or metal coordination can involve a large range of length scales, from molecular pair-wise associations to segregated microdomains.[4,5] Interestingly, it is possible to combine these distinct strategies, provided that the corresponding length scales strongly differ, which results in a hierarchical organization and complex dynamics.[6,7,8]

Covalent adaptable networks (CANs) essentially involve dynamic covalent cross-links at the molecular scale, and as such can easily combine multiple exchange chemistries[9], or also be combined with previously described supramolecular organisations[10,11] or phase separation.[8,12,13]

Most of them feature timescales for covalent exchanges much longer than segmental mobility, as a consequence, these materials display well separated thermomechanical transitions with distinct temperature dependences for i) the glass transition, related to cooperative motion at the segmental scale, and ii) non-correlated bond exchanges at the scale of network segments.[14,15] Although these two transitions can be tuned somewhat independently, high glass transition thermosetting materials are typically obtained from networks highly cross-linked or containing rigid aromatic or polyclic backbones, and their limited variety has restricted the development of high T_g CANs (above 140 °C) to a limited set of examples.[16,17,18] The ever-increasing dynamic chemistries implemented in covalent bond exchanges give rise in contrast to a very wide range of thermomechanical behaviors; reviews on associative and dissociative dynamic networks are reported in many complementary papers.[19–27] The two key features characterizing these dynamic networks are their relaxation dynamics and their effective cross-link densities, both can be thermally or photochemically[28] varied depending on the chemistry involved.

There are mainly two classes of exchangeable networks that constitute the realm of CANs. Vitrimers, based on associative exchange mechanisms maintain a constant connectivity regardless of temperature.[29] Set aside specific cases involving complex structuration of the materials (composites, microphase separation), the temperature dependence of their viscosity is solely controlled by the rate of exchange reactions and consequently varies weakly in accessible temperature ranges. In contrast, dissociative networks rely on the formation and disruption of adducts by exothermic equilibrated reactions and consequently show a decrease in cross-link density when temperature is increased. The temperature dependence of their viscosity, controlled both by the rate of exchange and the variation of cross-link density, is consequently much higher. A few systems based on dissociative exchanges demonstrating an intermediate behaviour typical

of associative CANs have also been recently reported.[21,27,30–34] Although being based on dissociative exchangeable cross-links as demonstrated by experiments on model compounds, the corresponding chemical equilibrium and cross-link density can remain unchanged in a large temperature range in which these specific CANs demonstrate rheological properties indiscernible from vitrimers. However, we have recently proposed a thorough rheological characterization methodology based on time-temperature superposed stress relaxation experiments (TTS-SR) that enables clearly differentiating and comparing all type of CANs,[14] emphasizing that in certain conditions dissociative networks might display a more advantageous balance between creep resistance at low temperatures and processability at high temperatures compared to purely associative CANs.

Modulating the viscosity profiles of CANs with temperature can thus be achieved through two distinct handles: i) the rate of chemical exchange reactions, and ii) the respective connectivity of permanent and transient bonds across the network. Understanding the interdependence between these two parameters is thus of paramount importance to understand the viscoelastic behaviour of dynamic networks and to define a clear set of rules to design and formulate CANs for dedicated applications. The recent review of Guerre, Winne, Du Prez and coworkers[22] details the many parameters that have been found, to-date, to alter the dynamics of CANs: i) internal and external catalysis including the variable stoichiometry of reactive groups, ii) chemical environment of the exchangeable reactions (solvent effect) affected by the nature of polymer backbone or possible phase separation, and iii) the topology of the networks that can be varied through the cross-link density, the presence of dangling chains or sol fraction as well as the combination of permanent and transient cross-links in copolymer or interpenetrated networks.[35] The effect of the last feature on the relaxation dynamics, that we consider as the most relevant in terms of generalizable design

rules as it is not related to any particular chemistry, follows however different trends depending on the system considered experimentally so far. It must also be noted that it is rather challenging to truly measure dynamics specifically due to network rearrangement and separate them from additional chemical and physical effects. Some studies focused on changing the stoichiometry of reactants to modify the network topology,[36] yet this strategy inevitably led to question whether variations of the dynamics are of chemical nature (reactivity variations of associative exchanges in which a rate-limiting bimolecular reaction step is involved and the corresponding reactants are present in various concentrations) or of purely topological nature.

Nicolaÿ and coworkers recently reacted short poly(1,2-butadiene)s with different contents of bis-dioxaborolane-functionalized dithiols acting as dynamic cross-linkers using thiol-ene chemistry.[37] They found that the dynamic networks with lower cross-link densities displayed considerably faster stress relaxation, with relaxation times varying from ca. 700 s to 130 s at 140 °C for networks obtained from linear precursors having an average of 7 and 3 functionalities per chain, respectively. *NB*: the corresponding number of units between dynamic cross-link are 10 and 24, respectively. Although they acknowledged that a considerable part of the overall stress relaxation was due to network defects (dangling chains or soluble fraction due to limited connectivity of the network), it remained challenging to distinguish their contributions from those of the dynamic exchanges of cross-links during stress relaxation experiments. Torkelson and coworkers,[38] synthesized thiol-epoxy polymer networks using an A_3+B_2 polyaddition strategy that incorporates different contents of alkylated (permanent) and diester (dynamic) segments resulting from the corresponding dithiol precursors. They found that fractions of dynamic diester segments above 60-80 mol% led to the percolation of dynamic bonds across the network and enabled complete stress relaxation. The corresponding relaxation times increased moderately with the

fraction of permanent alkylated segments, which tends to indicate faster stress relaxation for higher densities of dynamic cross-links and conflicts with the findings of Nicolaÿ and coworkers. Finally, Hayashi and coworkers synthesized polyesters ($M_n \sim 15$ kg mol^{-1}) bearing various amounts of pendent carboxylic acid groups, that were further cross-linked by catalysed epoxy-acid addition using bisepoxydes.[39] They found that the transesterification exchanges afforded faster stress relaxation for networks with higher cross-link densities. They later meticulously compared networks with the same chemical composition but different cross-link densities by curing the same carboxylic-acid side-functionalized polyester with various amounts of bis-epoxydes (elastically active cross-links) and mono-epoxydes (elastically inactive).[40] For networks comprising between 3.5 and 7 monomer units between cross-links, they found only weak differences between the relaxation dynamics of the networks.

Dissociative CANs having 1,2,3-triazolium cross-links constitute a particularly versatile platform as all difunctional building blocks (i.e. alkynes, azides and halides) are either commercially available or can be easily introduced on a broad variety of molecular or macromolecular precursors through highly efficient and selective chemical reactions. Polymer networks comprising 1,2,3-triazolium cross-links and either aliphatic,[41] polyether,[42] perfluoroether,[43] aromatic,[44] or polystyrene segments,[14] have been reported so far. Besides, we recently reported that the covalent exchange dynamics of the 1,2,3-triazolium cross-links were accelerated by a factor 50 in the case of polystyrene networks. This feature was attributed to the chemical structure of the exchangeable *N*-substituents of 1,2,3-triazolium cross-links, which consisted exclusively in benzylic groups.

The present manuscript aims at expanding further the scope of poly(1,2,3-triazolium) CANs obtained through AB+AB or AA+BB thermally initiated alkyne-azide cycloaddition (TAAC) and

investigating the correlations between the structural features of the resulting networks and their relaxation dynamics. Two key features were investigated: i) the introduction of heterocyclic and aromatic segments, that affords CANs with T_gs ranging from 46 to 146 °C, and ii) the structural variation of the exchangeable substituents at the *N*-1 and *N*-3 positions (aliphatic or benzylic groups) that enables achieving fast relaxation times (down to 30 s at 160 °C) while maintaining a thermomechanical behaviour typical of associative CANs. From the perspective of CAN design, thorough analysis of rheological experiments shows that at temperatures above T_g (that can reach as low as $T_g + 20$ °C), the relaxation dynamics in these 1,2,3-triazolium-based dissociative CANs are exclusively driven by the chemical structure of the *N*-substituents and do not depend on the chemical composition or topology of the polymer networks. However, we demonstrate that the topology of the networks, and more particularly the density of dynamic cross-links has a strong influence on the temperature-dependence of the cross-link density.

EXPERIMENTAL SECTION

Materials. Sodium azide (NaN$_3$, 99%), sodium hydride (NaH, 99%), propargyl bromide (80 wt% in toluene), 1,2-dibromoethane (>99%), potassium carbonate (>99%), 18-crown-6 (99%), 1,8-diiodooctane (**7**, 97%), 1,2-bis(2-iodoethoxy)ethane (**8**, 96%) and solvents (tetrahydrofuran (THF), ethyl acetate, petroleum ether, *N,N*-dimethylformamide (DMF), acetone, dichloromethane (DCM)) with the highest purity were purchased from Merck and used as received. 4-(Azidomethyl)benzyl alcohol **1**,[45] 4-(1-methyl-1-(4-prop-2-ynyloxy-phenyl)-ethyl)-phenol **3**,[46] α-azide-ω-alkyne 1,4:3,6-dianhydrohexitol **6**,[47] 1,6-bis(2-propyn-1-yloxy)hexane **9** and α,α'-diazido-*p*-xylene **10** were synthesized as reported previously.[48] *Please note that extreme caution is advised when handling organic azides with* $r_N = (n_C + n_O)/n_N$ *values ranging from 1 to 3 whereas compounds with* $r_N < 1$ *can be extremely instable and their isolation should be avoided*.[49]

Nuclear magnetic resonance. ^{1}H NMR (400 MHz) and ^{13}C NMR (100 MHz) spectra were recorded on Bruker Avance 300 or 400 spectrometers in CDCl$_3$ using a 5-mm QNP probe at 363 K. Chemical shifts (δ) are given in ppm in reference to residual hydrogenated solvent for ^{1}H NMR (δ = 7.26 ppm) and to deuterated solvent for ^{13}C NMR (δ = 77.0 ppm).

Thermal characterizations. Differential scanning calorimetry (DSC) was performed using a DSC Q200 (TA Instrument) calibrated with an indium standard. The samples were prepared using hermetic pans and the experiments were conducted under a helium purge of 25 mL min^{-1} on ca. 8 mg. The sample was first heated to 200 °C at a rate of 10 °C min^{-1} and isothermally annealed for 2 min. Then, the temperature was decreased to –80 °C at a rate of 10 °C min^{-1} followed by a second heating to 200 °C at a rate of 10 °C min^{-1}. The glass transition temperatures (T_g) were measured at the mid-point of the transition (on the second heating cycle) using the TA Thermal Analysis software. Thermogravimetric analysis (TGA) was performed using a TGA Q500 (TA

Instruments). A heating ramp from 20 to 600 °C was applied at 10 °C min^{-1} under a helium purge of 60 mL min^{-1} to ca. 8 mg.

X-ray photoelectron spectroscopy. X-ray photoelectron spectroscopy (XPS) experiments were carried out using a K-Alpha X-ray Photoelectron Spectrometer from Thermo Fisher Scientific equipped with a micro-focused mono-chromatic Al Kα X-ray beam source (1486.6 eV, 400 × 400 μm^2 spot size) and a flood gun to compensate for the static charge build-up. Ca. 200 μm thick slices of TPIL dynamic networks **11-14** were cut parallel to their surface using a razor blade and clipped on the sample holders. The samples were then outgassed in the fast entry airlock at $2 × 10^{-7}$ mbar before being transferred to the analysis chamber. All data were acquired at the normal with respect to the plane of the surface. High-resolution core-level spectra of C_{1s}, I_{3d}, N_{1s}, Si_{2p} were recorded with a 80 eV pass energy and 0.1 eV step size. The peaks were referenced to C_{1s} at 284.6 eV. The Avantage software was used for digital acquisition and data processing. The N_{1s} high definition spectra were fitted using a combination of Lorentzian and Gaussian line shapes. The details for data processing are described in the ESI.

Dynamic mechanical analysis. Dynamic mechanical analysis (DMA) was performed on a DMA Q800 (TA Instrument) in the tension film mode under a dry nitrogen atmosphere. Rectangular samples of 5.0 × 1.5 mm^2 cross-section and ca. 25 mm length were tested at a frequency of 1 Hz, an amplitude of 5 μm and a heating rate of 3 °C min^{-1} from –80 °C to 200 °C. T_α values were taken at the maximum value of the loss modulus. Elastic moduli at the rubbery plateau (G_0) were given as the value of E' at 150 °C.

Rheology. Rheological measurements were performed on a MARS 60 rheometer (ThermoScientific) using 8 mm melt-pressed disks glued to the geometries as previously described.[14] A succession of measuring steps within the linear viscoelastic domain were conducted

at temperatures above the T_g of TPIL dynamic networks ranging from 120 to 180 °C and involving for each temperature: equilibration for 30 min and stress relaxation experiments (0.5% strain for 1h). Construction of the relaxation master curve $\tilde{G}(t)$ at a common reference temperature $T_0 = 130$ °C was carried out by time-temperature superposition using $\tilde{G}(t, T_0) = b_T \cdot G(t/a_T, T)$ and a methodology previously described in details.[14]

Synthesis of 4-(2-propynyloxy)-benzyl azide 2. Sodium hydride (3.60 g, 150 mmol) was added in small portions to a stirred solution of 4-(azidomethyl)benzyl alcohol **1** (10.6 g, 65.0 mmol) and 18-crown-6 (20 mg, 0.08 mmol) in dry THF (80 mL) maintained at 0 °C under argon. After hydrogen was entirely emitted, propargyl bromide (14.5 mL, 130 mmol) was added dropwise. The mixture was stirred overnight at room temperature and after neutralization of residual NaH by adding distilled water (100 mL) THF was removed under reduced pressure. The aqueous suspension of the product was then extracted with DCM (4 × 250 mL). After drying the organic extracts with Na_2SO_4 and evaporation of the solvents under reduced pressure, the crude product was purified by flash chromatography eluting with a 96:4 mixture of petroleum ether and ethyl acetate to yield **2** as a slightly yellow liquid (10.3 g, 78.6 %). ^{1}H NMR ($CDCl_3$) δ (ppm): 7.38 (d, J = 8.1 Hz, C**H**-2, 2H), 7.31 (d, J = 8.1 Hz, C**H**-3, 2H), 4.62 (s, C**H**$_2$OCH$_2$C≡CH, 2H), 4.34 (s, C**H**$_2$N$_3$, 2H), 4.18 (d, J = 2.4 Hz, CH$_2$OC**H**$_2$C≡CH, 2H), 2.48 (t, J = 2.4 Hz, CH$_2$OCH$_2$C≡C**H**, 1H). ^{13}C NMR ($CDCl_3$) δ (ppm): 137.49 (**C**-4), 134.98 (**C**-1), 128.47 (**C**-3), 128.31 (**C**-2), 79.48 (CH$_2$OCH$_2$**C**≡CH), 74.72 (CH$_2$OCH$_2$C≡**C**H), 71.07 (**C**H$_2$OCH$_2$C≡CH), 57.19 (CH$_2$O**C**H$_2$C≡CH), 54.48 (**C**H$_2$N$_3$). HRMS (ESI) m/z: [M + Na]$^+$ calculated for $C_{11}H_{11}N_3NaO$, 224.0794; found, 224.0789.

Synthesis of α-bromide-ω-alkyne 4. Potassium carbonate (124 g, 900 mmol), 1,2-dibromoethane (77.6 mL, 900 mmol) and 18-crown-6 (50 mg, 0.2 mmol) were added to a solution of 4-[1-methyl-1-(4-prop-2-ynyloxy-phenyl)-ethyl]-phenol **3** (24.0 g, 90.1 mmol) in acetone (400 mL). The reaction mixture was refluxed under argon for 72 h, filtered and evaporated to dryness. The residue was extracted from water (25 mL) with dichloromethane (3 × 100 mL). After drying the organic extracts with Na_2SO_4 and evaporation of the solvents, the crude product was purified by flash chromatography eluting with a 9:1 mixture of petroleum ether and ethyl acetate to yield

4 as a white solid (26.3 g, 78.2%). ^{1}HNMR (CDCl$_3$) δ(ppm): 7.06 (d, J = 9.0 Hz, CH-3 and CH-7, 4H), 6.79 (d, J = 8.8 Hz, CH-8, 2H), 6.72 (d, J = 8.8 Hz, CH-2, 2H), 4.56 (d, J = 2.4 Hz, CH$_2$C≡CH, 2H), 4.17 (t, J = 6.2 Hz, CH$_2$CH$_2$Br, 2H), 3.52 (t, J = 6.2 Hz, CH$_2$CH$_2$Br, 2H), 2.42 (t, J = 2.4 Hz, CH$_2$C≡CH, 1H), 1.55 (s, CH$_3$, 6H). ^{13}CNMR (CDCl$_3$) δ(ppm): 155.85 (C-1), 155.39 (C-9), 143.84, 143.74 (C-4 and C-6), 127.79, 127.67 (C-3 and C-7), 114.15, 114.08 (C-2 and C-8), 78.74 (CH$_2$C≡CH), 75.34 (CH$_2$C≡CH), 67.77 (CH$_2$CH$_2$Br), 55.72 (CH$_2$C≡CH), 41.69 (C-5), 30.94 (CH$_3$), 29.21 (CH$_2$CH$_2$Br). HRMS (ESI) m/z: [M + Na]$^+$ calculated for C$_{20}$H$_{21}$BrNaO$_2$, 395.0617; found, 395.0610.

Synthesis of α-azide-ω-alkyne 5. α-Bromide-ω-alkyne **4** (26.3 g, 70.5 mmol) and sodium azide (13.7 g, 212 mmol) were added to a round-bottom flask containing DMF (250 mL). The mixture was stirred in the dark for 16 h at 60 °C. The solvent was evaporated under reduced pressure and the residue was extracted from water (50 mL) with ethyl acetate (3 × 200 mL). After drying the organic layers with Na$_2$SO$_4$, filtration and evaporation of the solvents under reduced pressure, the crude product was purified by flash chromatography eluting with a 9:1 mixture of petroleum ether and ethyl acetate to yield **5** as a white solid (16.4 g, 69.6%). ^{1}HNMR (CDCl$_3$) δ(ppm): 7.17 (d, J = 8.8 Hz, C**H**-3 and C**H**-7, 4H), 6.89 (d, J = 8.8 Hz, C**H**-8, 2H), 6.83 (d, J = 9.2 Hz, C**H**-2, 2H), 4.67 (d, J = 2.4 Hz, C**H**$_2$C≡CH, 2H), 4.13 (t, J = 5.0 Hz, C**H**$_2$CH$_2$Br, 2H), 3.58 (t, J = 5.0 Hz, CH$_2$C**H**$_2$Br, 2H), 2.52 (t, J = 2.4 Hz, CH$_2$C≡C**H**, 1H), 1.65 (s, CH$_3$, 6H). ^{13}CNMR (CDCl$_3$) δ(ppm): 156.03 (**C**-1), 155.41 (**C**-9), 143.90,143.69 (**C**-4 and **C**-6), 127.79,127.70 (**C**-3 and **C**-7), 114.17,113.93 (**C**-2 and **C**-8), 78.76 (CH$_2$**C**≡CH), 75.33 (CH$_2$C≡**C**H), 66.87 (**C**H$_2$CH$_2$N$_3$), 55.75 (**C**H$_2$C≡CH), 50.15 (CH$_2$**C**H$_2$N$_3$), 41.71 (**C**-5), 30.96 (**C**H$_3$). HRMS (ESI) m/z: [M + Na]$^+$ calculated for C$_{20}$H$_{21}$N$_3$NaO$_2$, 358.1526; found, 358.1516.

General procedure for the preparation of TPIL dynamic networks. Synthesis of 11. A fully miscible mixture of α-azide-ω-alkyne monomer **2** (1.91 g, 7.60 mmol) and 1,8-diiodooctane cross-linker **7** (695 mg, 1.90 mmol) was poured into a silicon mould and was gradually heated from 50 °C to 110 °C over a period of ca. 6h increasing the temperature by 5 °C increments every 30 minutes. The resulting ca. 2 mm thick network was unmoulded and annealed further under vacuum for 48 h at 110 °C in order to achieve equilibration of the material and to ensure complete curing of the system. TPIL dynamic network **11** was obtained as a transparent and homogeneous dark brown solid, and was cut into dimensions suited for rheological and thermomechanical measurements.

Synthesis of 12. The general procedure for the preparation of TPIL dynamic networks was applied to a mixture of α-azide-ω-alkyne **5** (2.20 g, 6.57 mmol) and 1,8-diiodooctane **7** (601 mg, 1.64 mmol) that was annealed for 24 h at 110 °C, 2 h at 130 °C and 2 h at 150 °C to yield **12** as a transparent and homogeneous yellow solid.

Synthesis of 13. The general procedure for the preparation of TPIL dynamic networks was applied to a mixture of α-azide-ω-alkyne monomer **6** (2.60 g, 12.4 mmol) and 1,2-bis(2-iodoethoxy)ethane cross-linker **8** (1.14 g, 3.10 mmol) that was annealed for 15 h at 110 °C, 2 h at 130 °C, and 30 min at 150 °C to yield **13** as a dark brown solid.

Synthesis of 14. The general procedure for the preparation of TPIL dynamic networks was applied to a mixture of diazide monomer **9** (1.16 g, 7.21 mmol), dialkyne monomer **10** (1.40 g, 7.21 mmol) and 1,8-diiodooctane cross-linker **7** (1.32 g, 3.60 mmol) that was annealed for 18 h at 80 °C, 24 h at 110 °C and 1 h at 130 °C to yield **14** as a dark red solid.
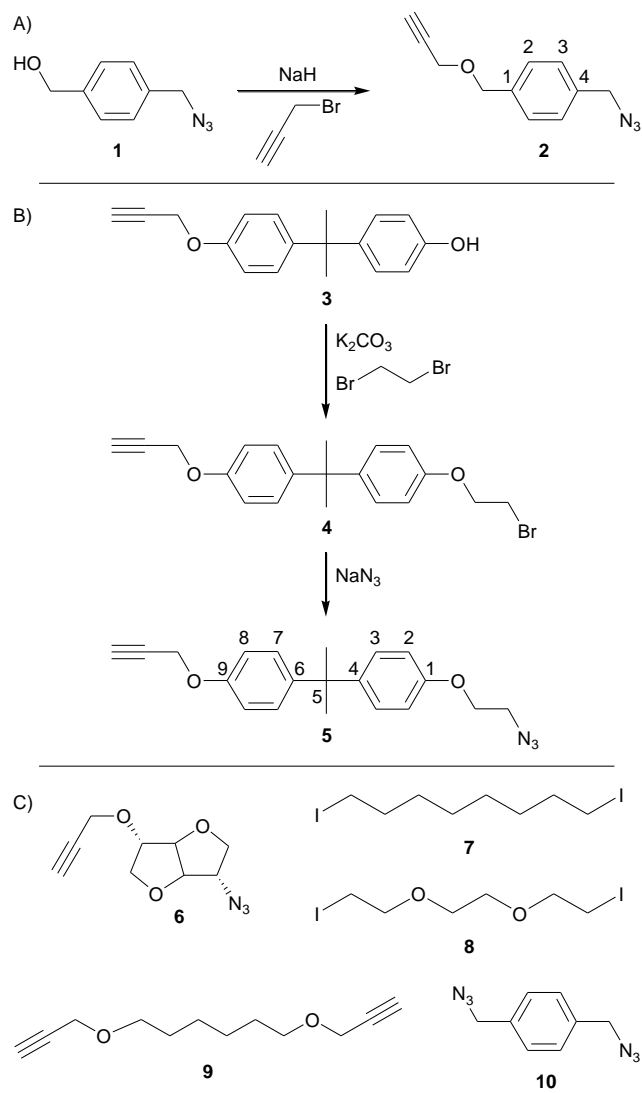
Scheme 1. A) Synthesis of α-azide-ω-alkyne **2**, B) synthesis of α-azide-ω-alkyne **5**, and C) chemical structures of α-azide-ω-alkyne **6**, cross-linkers **7**, **8**, dialkyne **9**, and diazide **10**.
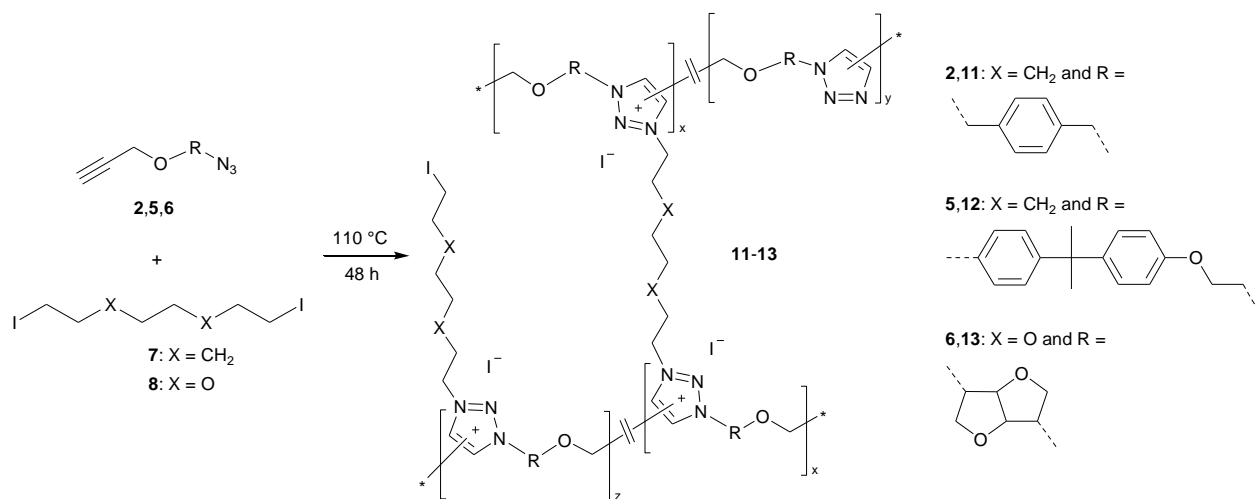
Scheme 2. Syntheses of TPIL dynamic networks **11-13**.
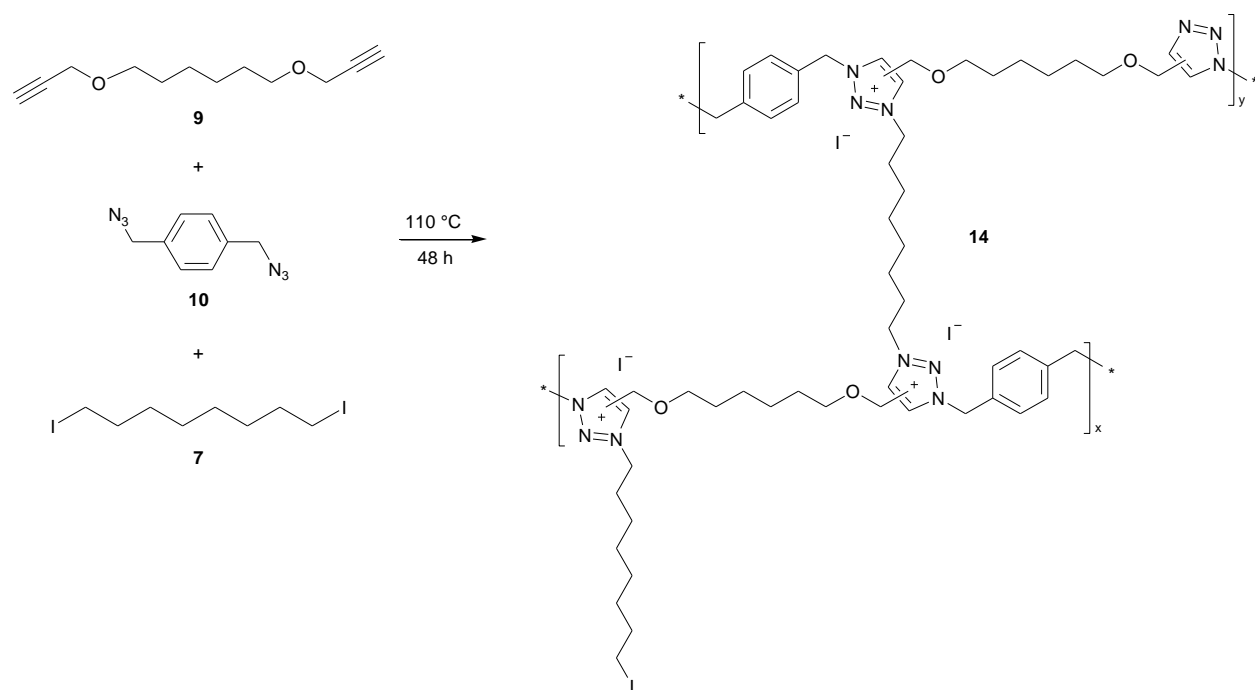
Scheme 3. Synthesis of TPIL dynamic network **14**.

16

RESULTS AND DISCUSSION

Synthesis of α-azide-ω-alkyne, dialkyne and diazide monomers. α-Azide-ω-alkyne monomer **2** was synthesized in 78.6% yield by *O*-alkylation of 4-(azidomethyl)benzyl alcohol **1** using propargyl bromide (**Scheme 1**). α-Azide-ω-alkyne monomer **5** was synthesized in two steps. First, *O*-alkylation of 4-[1-methyl-1-(4-prop-2-ynyloxy-phenyl)-ethyl]-phenol **3** using a tenfold excess of 1,2-dibromoethane afforded α-bromide-ω-alkyne precursor **4** in 78.2% yield. Further azidation of the bromomethylene group of **4** afforded α-azide-ω-alkyne monomer **5** in 69.6% yield. Compounds **2**, **4** and **5** were purified by column chromatography and as unprecedented compounds their structure and purity were confirmed by ^{1}H and ^{13}C NMR spectroscopy (**Fig. S1-S6 in the ESI†**) as well as by high-resolution electrospray ionization mass spectrometry. α-Azide-ω-alkyne monomer **6** was synthesized as described previously in three steps starting from isosorbide.[47] Dialkyne **9** and diazide **10** were synthesized in one step as described previously by *O*-alkylation and azidation of the corresponding diol and dibromide, respectively.[44] The purity and inherent stoichiometry of α-azide-ω-alkyne monomers **2**, **5** and **6** are crucial to maximize the polymerization degree (X_n) of the poly(1,2,3-triazole) intermediates involved in the synthesis of TPIL dynamic networks **11-13**. Stoichiometry between **9** and **10** was adjusted using ^{1}H NMR spectroscopy before preparation of TPIL dynamic network **14**.

Synthesis of TPIL dynamic networks 11–14. TPIL dynamic networks **11–14** were synthesized by solvent- and catalyst-free thermally initiated TAAC polyaddition using either AB+AB or AA+BB approaches and concomitant *N*-alkylation of the resulting linear poly(1,2,3-triazole) chains using diiodide cross-linkers (**Schemes 2 and 3**). Initially, TAAC polyaddition of α-azide-ω-alkyne monomers **2** and **5** in the presence of 1,8-diiodooctane cross-linker **7** afforded TPIL dynamic networks **11** and **12**, respectively. Since isosorbide-based α-azide-ω-alkyne

monomer **6** and 1,8-diiodooctane **7** are not miscible and that the use of co-solvents for synthesizing CANs is highly undesirable, TPIL dynamic network **13** was obtained from a miscible mixture of α-azide-ω-alkyne monomer **6** and 1,2-bis(2-iodoethoxy)ethane cross-linker **8**. Finally, TPIL dynamic network **14** was obtained by TAAC polyaddition between a stoichiometric amount of dialkyne **8** and diazide **10** in the presence of 1,8-diiodooctane cross-linker **7** (**Scheme 3**). In all cases the ratio between precursors of 1,2,3-triazole (i.e. 1:1 azide and alkyne functionalities) and iodide groups was equal to 0.5. Due to the highly exothermic nature of the TAAC polyaddition reaction (ΔH ranges from -250 to -200 kJ mol^{-1}),[47] the synthesis of TPIL dynamic networks **11–14** was carried out by cautiously increasing the curing temperature from 50 °C to 110 °C by ca. 5 °C increments every 30 min. ***CAUTION!*** This progressive heating procedure is strongly suggested as a direct heating of these azide-containing reactive mixtures at 110 °C may induce thermal runaway and carbonization of the samples. Azide-containing monomers involved in the synthesis of TPIL dynamic networks **11–14** can be considered as rather stable at room temperature, i.e. $r_N = (n_C + n_O)/n_N = 4.00$, 7.33, 4.00 and 1.33 for **2**, **5**, **6** and **10**, respectively. Even after significant dilution with the cross-linker (and also the dialkyne comonomer in the case of the most reactive diazide monomer **10**), the direct heating at ca. 110 °C of multi-gram batches could occasionally induce a thermal runaway. Once a conversion past the gel point was reached, TPIL dynamic networks **11-14** were unmoulded, further cured above their glass transition temperature (T_g) for 24h to 48h and finally obtained as homogeneous solids with colours ranging from orange to dark brown (**Fig. 1**). The full consumption of azide groups after full curing of TPIL dynamic networks **11-14** was verified by ATR-FTIR (**Fig. S7** in ESI†) through the total disappearance of the intense asymmetric stretching vibration band of azide groups at ca. 2100 cm^{-1}.
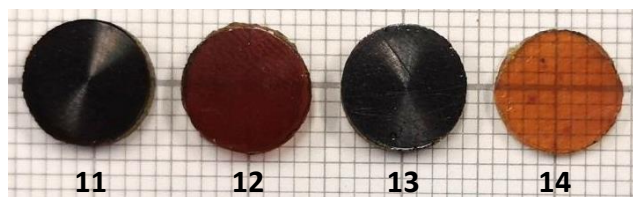
Fig. 1 Optical images of ca. 2 mm thick TPIL dynamic networks **11**–**14** (Dimensions of the tiles are 0.5×0.5 cm^2).

Resulting TPIL dynamic networks **11-14** are amorphous materials having T_g values reasonably well correlated to the rigidity of the monomers involved in their synthesis (**Table 1**). BPA- and isosorbide-based units are known for their high stiffness,[50] and consequently afforded high T_g values of 119 and 146 °C for samples **12** and **13**, respectively. Xylylene-based monomer **2** led to a lower T_g value of 84 °C for TPIL **11**. TPIL **14** comprising flexible aliphatic dialkyne **10** displayed an even lower T_g value of 48 °C. TPIL dynamic networks **11**–**14** exhibit comparable TGA profiles (**Fig. S8 in the ESI†**), with temperatures at 10% weight loss (T_{d10}) in the 250–270 °C range, in par with those previously observed for networks having 1,2,3-triazolium cross-links ($T_{d10} \sim 235$–340 °C),[14,21,41,43,44] or more generally for linear poly(1,2,3-triazolium iodides) ($T_{d10} \sim 200$–255 °C).[51] It must however be noted that the effective thermal stability in the 170-200 °C range is significantly lower for isosorbide-based TPIL **13**, that undergoes carbonization and foaming over a few hours above 175 °C (**Fig. S9 in the ESI†**). It is worth noting that all TPIL networks led to significant ash residues at 600 °C, i.e. 27, 15, 31 and 12 wt% for **11-14**, respectively.

Extent of *N*-alkylation reaction in TPIL dynamic networks 11−14. The extents of *N*-alkylation reaction (*x*) after curing of TPIL dynamic networks **11–14,** which are related to the cross-link density and the curing efficiency, were determined by XPS analysis and fitting of the high resolution N_{1s} spectra (**Fig. 2**).[21] In previous XPS analyses of 1,2,3-triazolium networks from our group,[21,41] we were able to properly attribute the binding energies of different N_{1s} signals of 1,2,3-triazole and 1,2,3-triazolium groups using model compounds. In the present networks displaying a much wider variety of *N*-substituents, we had to resort to a more global fitting method. The peak fitting (continuous lines in **Fig. 2**) was thus realized using Origin 2018 software by assigning 6 Gaussian functions (corresponding to the different nitrogen atoms of 1,2,3-triazole and 1,2,3-triazolium groups), centered on fully adjustable and independent binding energies, with a unique width, and identical areas for the three 1,2,3-triazole and the three 1,2,3-triazolium nitrogen signals. In all cases, it was found that three Gaussians were centered within the 403-401 eV range characteristic of 1,2,3-triazolium groups while the remaining three Gaussians were centered within the 400-398 eV range characteristic of 1,2,3-triazole groups. Also, in all cases the peak fitting resulted in the exact overlap of two Gaussians for 1,2,3-triazoles. The extent of *N*-alkylation reaction *x* was thus calculated from the fractions of 1,2,3-triazolium (T⁺) and 1,2,3-triazole (T) groups (α) and the stoichiometric ratio of alkylating agents to azide/alkyne groups (*z* = 0.5) using equation 1:

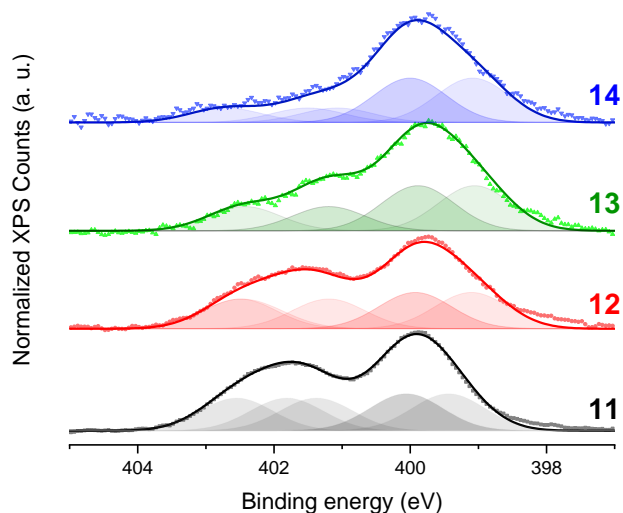$$x = \alpha/z = 2[\text{T}^+]/([\text{T}^+]+[\text{T}]) \tag{1}$$

Fig. 2 High resolution N_{1s} spectra of TPIL dynamic networks **11**–**14**. The spectra are shifted vertically for clarity. The extents of *N*-alkylation reaction (*x*) are calculated from the 1,2,3-triazolium:1,2,3-triazole area ratios as discussed in the text (eq. 1). Please note that overlapping of Gaussian signals are indicated by darker shades.

TPIL dynamic networks **11** and **12** displayed high level of cross-linking with extents of *N*-alkylation reaction above 90% in good agreement with previously described TPIL dynamic networks.[21,41] TPIL dynamic network **13** exhibited however a significantly lower extent of *N*-alkylation approaching 70%. This is most likely due to the premature occurrence of vitrification during network curing as the limited thermal stability of TPIL dynamic network **13** impeded to cure the sample at a temperature high enough compared to T_g (*i.e.* 150 and 146 °C for the curing temperature and T_g, respectively). Surprisingly, XPS characterization of TPIL dynamic network **14** exhibited an even lower extent of *N*-alkylation reaction of about 50%.

Thermomechanical properties of TPIL dynamic networks 11–14. Thermomechanical properties of TPIL dynamic networks **11-14** were initially assessed by DMA (**Fig. 3**). Samples **11-13** display T_α temperatures in fair agreement with T_g values measured by DSC (**Table 1**), as well

as symmetric and monomodal tan(δ) profiles as characteristic features of homogeneously cross-linked polymer networks. The corresponding plateau moduli up to 170 °C ($E'_{plateau}$ = 4–14 MPa) are typical features of highly cross-linked glassy polymer materials (**Table 1**). The decrease of storage moduli upon further heating observed for samples **11** and **12** have been also reported for other dissociative CANs exhibiting vitrimer-like properties.[14,30,52] TPIL dynamic network **14** that showed the lowest extent of N-alkylation by analysis of XPS experiments still behaves as a highly cross-linked elastomer ($E'_{plateau}$ = 6.7 MPa) but displays a dual transition and an asymmetric tan(δ) profile, most likely indicative of an heterogeneous network with broad distribution of cross-link densities. Possible phase separation of poly(1,2,3-triazole) chains and cross-linker **7** at the early stage of the curing might explain such an heterogeneous distribution of the cross-linker in the sample, and could also explain the lower overall extent of N-alkylation reaction calculated from XPS data.
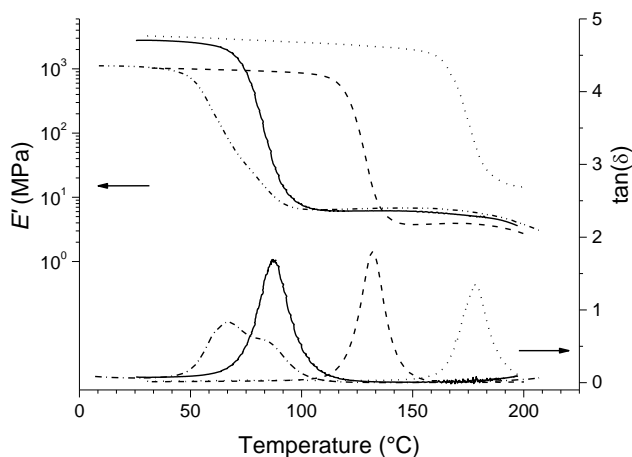

Fig. 3 DMA traces (1 Hz, 3 °C min⁻¹) of TPIL dynamic networks **11** (solid lines), **12** (dashed lines), **13** (dotted lines) and **14** (dash-dotted lines).

Viscosity profiles of TPIL dynamic networks 11, 12 and 14. The dynamics of network relaxations for samples **11**, **12** and **14** were analyzed by performing stress relaxation experiments at temperatures from ca. 20 °C above T_g up to 180 °C, and by building relaxation master curves using previously described time-temperature superposition (TTS) (**Fig. 4** and **Fig. S10, S11 in the ESI†** for samples **11, 12** and **14**, respectively). The temperature dependent dynamic properties of sample **13** could not be properly characterized due to the narrow temperature range located above T_g and below the degradation temperature. Obtained results for **11, 12** and **14** were compared to previously reported aliphatic and styrenic TPIL dynamic networks **15** and **16**, respectively (**Scheme S1 in the ESI†**).[14,41]

The non-normalized stress relaxation moduli (**Fig. 4a**, **S10a** and **S11a in the ESI†**) show well-defined plateau moduli and as expected relaxation times decreasing with increasing temperature. These relaxation moduli can be shifted through a TTS (using a common reference temperature T_0 = 130 °C for all samples) to construct well defined relaxation master curves, at least for samples **11** and **12** over the whole temperature range probed (i.e. 115 °C – 175 °C and 130 °C – 175 °C, resp.), and for sample **14** from 100 °C to 145 °C (**Fig. 4b, S10b** and **S11b in the ESI†**). The proper superposition of stress relaxation curves in these temperature ranges indicates a common relaxation mechanism that we can confidently attribute to covalent exchanges of the 1,2,3-triazolium cross-links. The shift factors a_T and b_T enable thus to determine with good accuracy the temperature dependency of relaxation times and zero-shear moduli, respectively (**Fig. 4c, S10c** and **S11c in the ESI†**). Therefore, it was found that the a_T shift factors of the dynamic networks all follow an Arrhenius dependence, and that the corresponding *kinetic* activation energies $E_{a,\tau}$ range from 126 to 135 kJ mol^{-1}.

Table 1. Chemical and physical properties of TPIL dynamic networks **11-14**.

N°	x [a] (%)	T_{d10} [b] (°C)	T_g [c] (°C)	T_α [d] (°C)	E' [e] (MPa)	G_0 [f] (MPa)	β [g]	$<\tau>$ [h] (s)	$E_{a,\tau}$ [i] (kJ mol^{-1})
11	93	250	84	73	6.1	2.5	0.71	100	126
12	90	270	119	120	3.8	1.0	0.81	4800	135
13	70	270	146	169	-	-	-	-	-
14	49	235	46	55	6.7	2.4	0.66	110	131

[a] Extent of the N-alkylation reaction determined by XPS; [b] Temperature for 10% weight loss determined by TGA; [c] Glass transition temperature determined by DSC; [d] Alpha transition temperature determined by DMA; [e] Elastic modulus at the rubbery plateau (in the 150-160 °C range depending on the sample) determined by DMA; [f] Plateau shear modulus determined from rheology (small amplitude oscillations); [g,h] Breadth of distribution, and average value of relaxation times at 150 °C determined by fitting of the stress relaxation master curves (see eqn. 2); [i] Kinetic activation energy determined from a_T shifts of SR-TTS.
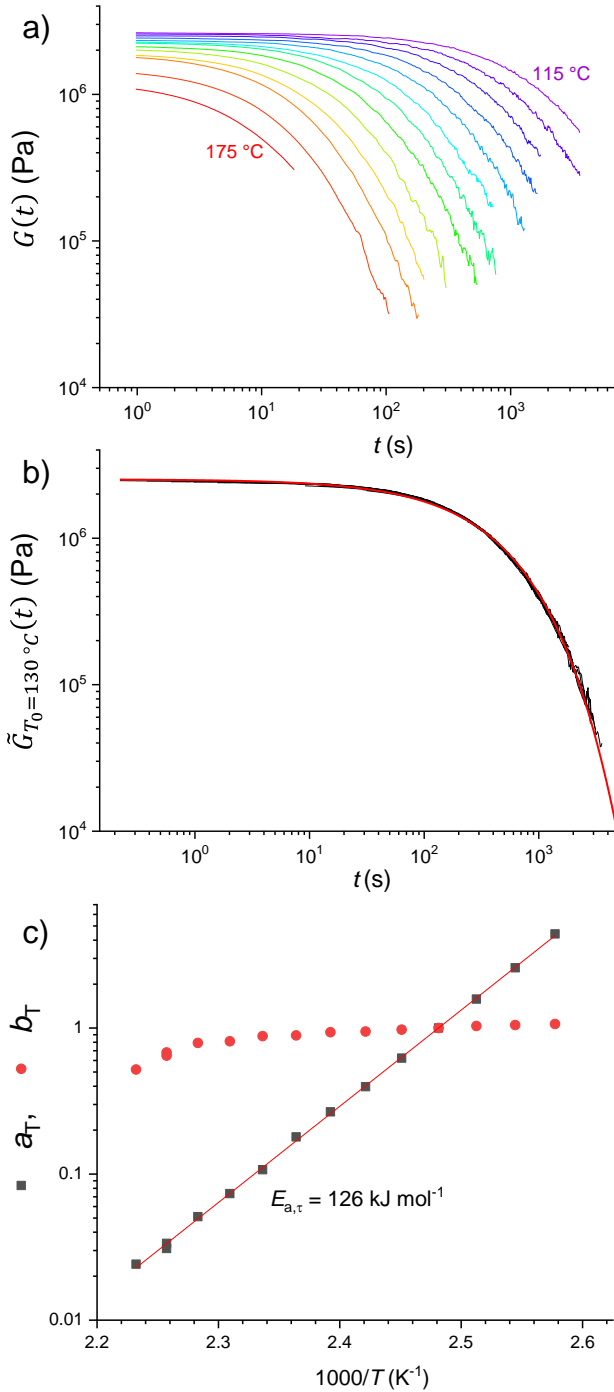
Fig. 4 a) Variable-temperature stress relaxation moduli of TPIL dynamic network **11** (from purple to red: 115 to 175 °C by +5 °C increments), and corresponding b) master curve and c) shift factors constructed at a reference temperature of $T_0 = 130$ °C. The red line in b) corresponds to a stretched exponential model (equation 2).

The b_T shift factors of samples **11**, **12** and **14** remain almost constant below 160 °C with values ranging from 0.8 to 1.0, essentially indicating that the cross-link density does not vary appreciably within this temperature range. However, above 160 °C samples **11** and **14** demonstrate a noticeable decrease in b_T shift factors and thus in cross-link density.
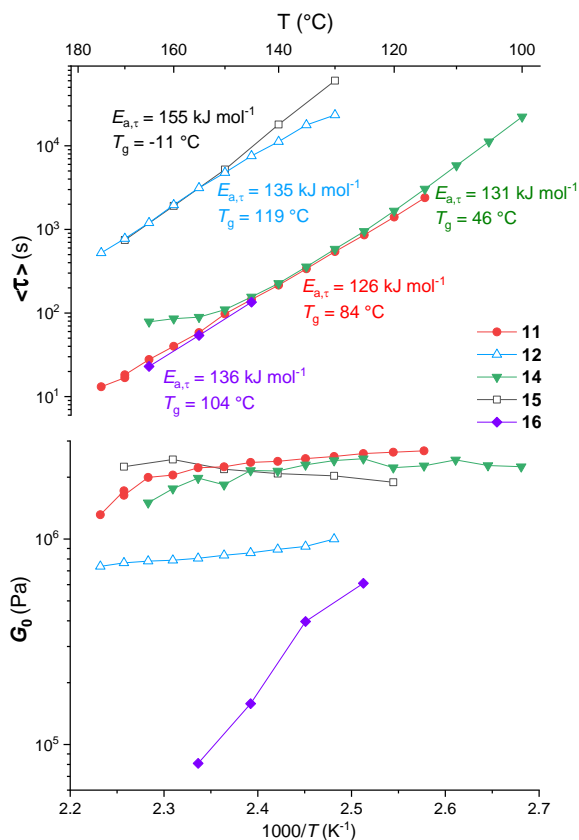

Fig. 5 Temperature dependence of top) the average relaxation times and bottom) zero-shear moduli for TPIL dynamic networks **11** (red solid circles), **12** (blue open triangles), **14** (green solid triangles). Additional data for previously reported aliphatic TPIL dynamic network **15** (black open squares) and polystyrene-based TPIL dynamic network **16** (purple solid diamonds) have been added for comparison.[21,41].

All master curves $\tilde{G}(t)$ could be reasonably well fitted using a stretched exponential model described by equation 2:

$$\tilde{G}(t) = \tilde{G}_0 e^{-\left(\frac{t}{\tau^*}\right)^{\beta}}$$

(2)

with β the breadth of distribution of the relaxation times. The average relaxation times <*τ*> and the zero-shear moduli at all temperatures can thus be extracted from these parameters[33] and the shift factors using equations 3 and 4:

$$\langle \tau \rangle (T) = \tau^*.a_T.\Gamma\left(\frac{1}{\beta}\right)/\beta$$

(3)

$$G_0(T) = \widetilde{G_0}.b_T$$

(4)

The evolutions of <*τ*> and G_0 as a function of reciprocal temperature are reported in **Fig. 5** for TPIL dynamic networks **11**, **12** and **14** as well as previously reported TPIL dynamic networks **15** (non-regioregular 1,2,3-triazolium cross-links having aliphatic *N*-substituents[21]) and **16** (regioregular 1,2,3-triazolium cross-links having benzylic *N*-substituents[14]). The kinetics activation energies $E_{a,\tau}$ were calculated from the a_T parameters using equation 5:

$$a_T \propto e^{\frac{E_{a,\tau}}{RT}}$$

(5)

In order to establish a precise correlation between the chemical structures of TPIL dynamic networks and their rheological properties, the various chemical structures of the different regioisomers constituting the dissociative 1,2,3-triazolium cross-links are represented in **Scheme 4**. The effective number of monomer units between cross-link, r_X, is calculated from the stoichiometry of the reactants and the extent of *N*-alkylation reaction *x* obtained from XPS measurements using equation 1. Also, as TPIL dynamic networks **11**, **12**, **14** and **15** are obtained by copper-free TAAC polyaddition, they contain a ca. 1:1 mixture of 1,3,4- and 1,3,5-trisubstituted 1,2,3-triazolium cross-links. However, as the 1,2,3-triazole-functionalized polystyrene precursor

of sample **16** is obtained by CuAAC this particular sample contains exclusively 1,3,4-trisubstituted 1,2,3-triazolium cross-links.

The temperature dependence of the relaxation times of TPIL dynamic networks **12** and **15**, having only aliphatic *N*-substituents at the 1,2,3-triazolium cross-links (**Scheme 4**), follow similar evolutions with comparable kinetic activation energies and average relaxation times at 150 °C of ca. 4800 s (**Figure 5a**). The deviation from Arrhenius behavior for **12** at temperatures below 140 °C may be due to experimental issues during the stress relaxation experiments when approaching the glass transition temperature (T_g = 119 °C). Indeed one would rather expect vitrification phenomena to slow down exchange kinetics and thus increase the network relaxation times. Also, TPIL dynamic networks **11** and **14** having a ca. 1:1 ratio of benzylic and aliphatic *N*- substituents and TPIL **16** having exclusively benzylic *N*-substituents at the 1,2,3-triazolium cross-links display identical relaxation times, i.e. ca. 50 times faster than for TPIL networks **12** and **15**, (about 100 s at 150 °C). It can thus be concluded that the overall relaxation times in these networks are essentially dictated by the fastest *N*-substituents at the 1,2,3-triazolium cross-links. This assertion remains valid even when the cross-link topology significantly differs as TPIL dynamic networks **11**, **14** and **16** comprise one dynamic cross-link every ca. 2, 4 and 10 repeat unit, respectively.

The temperature dependence of G_0 enables however to put in evidence three distinct behaviors within this series of TPIL dynamic networks (**Fig. 5b**). TPIL dynamic networks **12** and **15** that contain exclusively slower exchangeable aliphatic *N*-substituents (**Scheme 4**) display cross-link densities varying by a factor 1.2 and 1.3 between 120 and 180 °C, i.e. a nearly constant profile comparable to associative CANs. TPIL dynamic networks **11** and **14** containing one faster benzylic *N*-substituent per 1,2,3-triazolium cross-link also exhibit similar properties up to 160 °C but a noticeable decrease of cross-link density above that threshold. TPIL dynamic network **16**

containing two benzylic *N*-substituents per 1,2,3-triazolium cross-link, and a significantly lower cross-link density compared to other networks from the series exhibits however a drastic decrease of cross-link density above 120 °C a rheological signature typical of dissociative CANs.
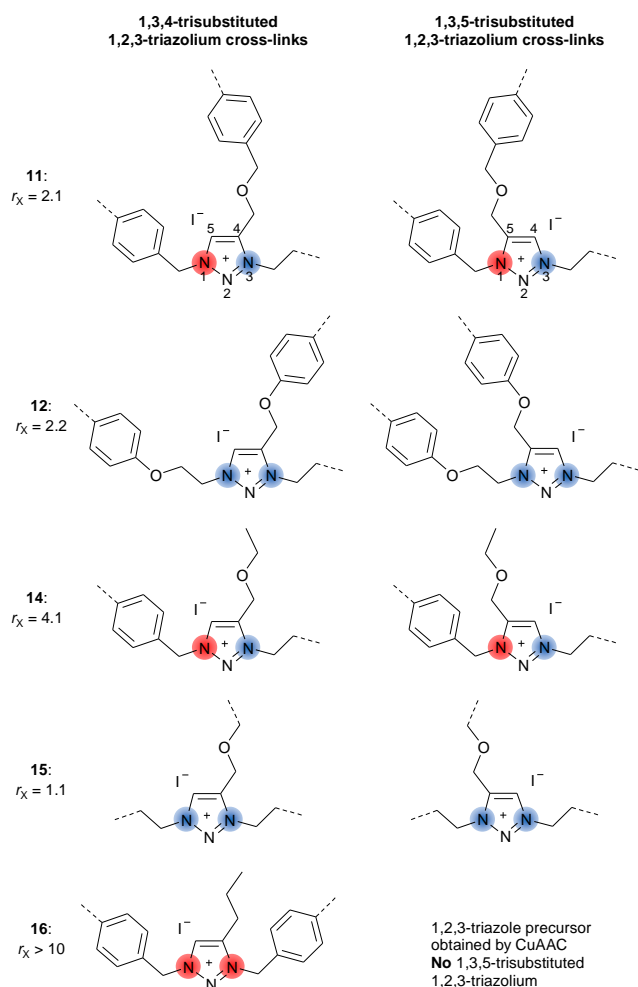
Scheme 4 Representation of the different regioisomers of 1,2,3-triazolium cross-links involved in TPIL dynamic networks **11**, **12**, **14**–**16** highlighting the various exchangeable *N*-substituents: faster benzylic *N*-substituents highlighted by red circles and slower aliphatic *N*-substituents highlighted by blue circles. r_X is the effective number of monomer units between cross-link.

CONCLUSIONS

We have demonstrated the versatility and extended the structural variety of the TPIL dynamic networks platform by synthesizing a series of networks including rigid heterocyclic or aromatic building blocks that can achieve T_gs as high as 146 °C. We also have shown that the careful design of the substituents at the N-1 and N-3 positions of 1,2,3-triazolium cross-links is critical to reach a favorable compromise between fast exchange kinetics and moderate temperature dependence of the cross-link density, a typical attribute of associative CANs. Most importantly we have distinguished three types of rheological behaviors depending on the chemical structure of the exchangeable substituents located at the N-1 and N-3 positions of the 1,2,3-triazolium cross-links: i) two aliphatic N-substituents afford slow exchange kinetics and low temperature-dependence of G_0 indiscernible from associative CANs, ii) two benzylic N-substituents afford fast exchange kinetics and extensive temperature-dependence of G_0 typical of dissociative CANs, and iii) the combination of an aliphatic and a benzylic N-substituents affords a favorable compromise and combines the benefits of the two latter with fast relaxation times of ca. 100 s at 150 °C as in ii) and a minimal reduction of the cross-link density with the temperature increase as in i). This clearly highlights that different combinations of distinct N-substituents at the 1,2,3-triazolium cross-links have a major impact on the networks dynamics. However, the impact of regiochemistry and position of these different substituents is still an important question that remains. Further work is currently ongoing to solve this question and provide a precise structure/property relationship between exchange kinetics and chemical environment of the 1,2,3-triazolium cross-links.

In a more general aspect these results also enable one to draw a few conclusions that may have important implications in the advanced design of CANs to meet viscosity profiles required for cutting-edge applications. We found that above their T_g the relaxation time profiles of TPIL networks were exclusively determined by the chemical structure of the dynamic cross-links, and

did not significantly vary with the chemical composition of the surrounding polymer network. This provides further challenges to tune the chemical environment of the 1,2,3-triazolium coross-links. However, the evolution of the cross-link density with temperature, which is the second parameter that can be used to modulate the viscosity profiles in the case of dissociative CANs, appears strongly affected by the topology of the networks and notably by the density of dynamic cross-links. Consequently, this powerful and versatile handle that can in most cases be varied independently of the exchange chemistry at stakes offers wide possibilities to control the viscosity dependence and tune the reprocessability of CANs. Proper combination of high T_gs, fast relaxations and most importantly precise control over temperature dependence of the cross-link density should contribute to the development of next generation CANs.

ASSOCIATED CONTENT

Supporting Information. : ^{1}H and ^{13}C NMR of **2**, **4** and **5**, ATR-FTIR, TGA and rheological characterization of TPIL dynamic networks **11**–**14**.

AUTHOR INFORMATION

Corresponding Authors

* eric.drockenmuller@univ-lyon1.fr, damien.montarnal@univ-lyon1.fr.

Author Contributions

The manuscript was written through contributions of all authors. All authors have given approval to the final version of the manuscript.

Notes

The authors declare no competing financial interest.

REFERENCES

(1)   Pascault, J.-P.; Sautereau, H.; Verdu, J.; Williams, R. J. J. *Thermosetting Polymers*; CRC Press, 2002.

(2)   Post, W.; Susa, A.; Blaauw, R.; Molenveld, K.; Knoop, R. J. I. A Review on the Potential and Limitations of Recyclable Thermosets for Structural Applications. *Polym. Rev.* **2020**, *60* (2), 359–388.

(3)   *Handbook of Thermoplastic Elastomers*; Drobny, J. G., Ed.; Elsevier, 2014.

(4)   Wang, S.; Urban, M. W. Self-Healing Polymers. *Nat. Rev. Mater.* **2020**, *5* (8), 562–583.

(5)   Voorhaar, L.; Hoogenboom, R. Supramolecular Polymer Networks: Hydrogels and Bulk Materials. *Chem. Soc. Rev.* **2016**, *45* (14), 4013–4031.

(6)   Montarnal, D.; Delbosc, N.; Chamignon, C.; Virolleaud, M.-A.; Luo, Y.; Hawker, C. J.; Drockenmuller, E.; Bernard, J. Highly Ordered Nanoporous Films from Supramolecular Diblock Copolymers with Hydrogen-Bonding Junctions. *Angew. Chemie Int. Ed.* **2015**, *54* (38), 11117–11121.

(7)   Hentschel, J.; Kushner, A. M.; Ziller, J.; Guan, Z. Self-Healing Supramolecular Block Copolymers. *Angew. Chemie - Int. Ed.* **2012**, *51* (42), 10561–10565.

(8) Ricarte, R; Tournilhac, F.; Cloitre, M.; Leibler, L. Linear Viscoelasticity and Flow of Self-Assembled Vitrimers: The Case of a Polyethylene/Dioxaborolane System. *Macromolecules* **2020**, *53* (5), 1852–1866.

(9)   El-Zaatari, B. M.; Ishibashi, J. S. A.; Kalow, J. A. Cross-Linker Control of Vitrimer Flow. *Polym. Chem.* **2020**, *11* (33), 5339–5345.

(10)   Niu, X.; Wang, F.; Kui, X.; Zhang, R.; Wang, X.; Li, X.; Chen, T.; Sun, P.; Shi, A. C. Dual Cross-Linked Vinyl Vitrimer with Efficient Self-Catalysis Achieving Triple-Shape-Memory Properties. *Macromol. Rapid Commun.* **2019**, *40* (19), 1–8.

(11)   Martin, R.; Rekondo, A.; Ruiz De Luzuriaga, A.; Cabañero, G.; Grande, H. J.; Odriozola, I. The Processability of a Poly(Urea-Urethane) Elastomer Reversibly Crosslinked with Aromatic Disulfide Bridges. *J. Mater. Chem. A* **2014**, *2* (16), 5710–5715.

(12)   Lessard, J. J.; Scheutz, G. M.; Sung, S. H.; Lantz, K. A.; Epps, T. H.; Sumerlin, B. S. Block Copolymer Vitrimers. *J. Am. Chem. Soc.* **2020**, *142* (1), 283–289.

(13)   Ishibashi, J.; Fang, Y.; Kalow, J. Exploiting Block Copolymer Phase Segregation to Tune Vitrimer Properties. **2019**. https://doi.org/10.26434/chemrxiv.10000232.

(14)   Jourdain, A.; Asbai, R.; Anaya, O.; Chehimi, M. M.; Drockenmuller, E.; Montarnal, D. Rheological Properties of Covalent Adaptable Networks with 1,2,3-Triazolium Cross-Links: The Missing Link between Vitrimers and Dissociative Networks. *Macromolecules*. 2020, pp 1884–1900.

(15)   Capelot, M.; Unterlass, M. M.; Tournilhac, F.; Leibler, L. Catalytic Control of the Vitrimer Glass Transition. *ACS Macro Lett.* **2012**, *1* (7), 789–792.

(16) Liu, T; Hao, C.; Zhang, S.; Yang, S. ; Wang, L. ; Han, J. ; Li, Y.; Xin, J.; Zhang, J. A Self-Healable High Glass Transition Temperature Bioepoxy Material Based on Vitrimer Chemistry. *Macromolecules* **2018,** *51* (15), 5577-5585.

(17) Brunet, J.; Collas, F.; Humbert, M.; Perrin, L.; Brunel, F.; Lacôte, E.; Montarnal, D.; Raynaud, J. High Glass-Transition Temperature Polymer Networks Harnessing the Dynamic Ring Opening of Pinacol Boronates. *Angew. Chemie – Int. Ed.* **2019**, 58 (35), 12216–12222.

(18) Giebler, M.; Sperling, C.; Kaiser, S.; Duretek, I.; Schlögl, S. Epoxy-Anhydride Vitrimers from Aminoglycidyl Resins with High Glass Transition Temperature and Efficient Stress Relaxation. *Polymers* **2020**, *12* (5), 1148.

(19) Chakma, P.; Konkolewicz, D. Dynamic Covalent Bonds in Polymeric Materials. *Angew. Chemie - Int. Ed.* **2019**, *58* (29), 9682–9695.

(20) Jiang, Z.; Bhaskaran, A.; Aitken, H. M.; Shackleford, I. C. G.; Connal, L. A. Using Synergistic Multiple Dynamic Bonds to Construct Polymers with Engineered Properties. *Macromol. Rapid Commun.* **2019**, *40* (10), 1900038.

(21) Obadia, M. M.; Jourdain, A.; Cassagnau, P.; Montarnal, D.; Drockenmuller, E. Tuning the Viscosity Profile of Ionic Vitrimers Incorporating 1,2,3-Triazolium Cross-Links. *Adv. Funct. Mater.* **2017**, *27* (45), 1703258.

(22) Guerre, M.; Taplan, C.; Winne, J. M.; Du Prez, F. E. Vitrimers: Directing Chemical Reactivity to Control Material Properties. *Chem. Sci.* **2020**, *11* (19), 4855–4870.

(23) Van Zee, N. J.; Nicolaÿ, R. Vitrimers: Permanently Crosslinked Polymers with Dynamic Network Topology. *Prog. Polym. Sci.* **2020**, *104*, 101233.

(24) Winne, J. M.; Leibler, L.; Du Prez, F. E. Dynamic Covalent Chemistry in Polymer Networks: A Mechanistic Perspective. *Polym. Chem.* **2019**, *10* (45), 6091–6108.

(25) McBride, M. K.; Worrell, B. T.; Brown, T.; Cox, L. M.; Sowan, N.; Wang, C.; Podgorski, M.; Martinez, A. M.; Bowman, C. N. Enabling Applications of Covalent Adaptable Networks. *Annu. Rev. Chem. Biomol. Eng.* **2019**, *10*, 175–198.

(26) Scheutz, G. M.; Lessard, J. J.; Sims, M. B.; Sumerlin, B. S. Adaptable Crosslinks in Polymeric Materials: Resolving the Intersection of Thermoplastics and Thermosets. *J. Am. Chem. Soc.* **2019**, *141* (41), 16181–16196.

(27)   Elling, B. R.; Dichtel, W. R. Reprocessable Cross-Linked Polymer Networks: Are Associative Exchange Mechanisms Desirable? *ACS Cent. Sci.* **2020**, *6*, 1488−1496.

(28)   Worrell, B. T.; McBride, M. K.; Lyon, G. B.; Cox, L. M.; Wang, C.; Mavila, S.; Lim, C. H.; Coley, H. M.; Musgrave, C. B.; Ding, Y.; Bowman, C. N. Bistable and Photoswitchable States of Matter. *Nat. Commun.* **2018**, *9* (1), 2804.

(29)   Montarnal, D.; Capelot, M.; Tournilhac, F.; Leibler, L. Silica-like Malleable Materials from Permanent Organic Networks. *Science* **2011**, *334* (6058), 965–968.

(30)   Chakma, P.; Morley, C. N.; Sparks, J. L.; Konkolewicz, D. Exploring How Vitrimer-like Properties Can Be Achieved from Dissociative Exchange in Anilinium Salts. *Macromolecules* **2020**, *53* (4), 1233–1244.

(31)   Zhang, L.; Rowan, S. J. Effect of Sterics and Degree of Cross-Linking on the Mechanical Properties of Dynamic Poly(Alkylurea-Urethane) Networks. *Macromolecules* **2017**, *50* (13), 5051–5060.

(32)   Chen, X.; Li, L.; Jin, K.; Torkelson, J. M. Reprocessable Polyhydroxyurethane Networks Exhibiting Full Property Recovery and Concurrent Associative and Dissociative Dynamic Chemistry: Via Transcarbamoylation and Reversible Cyclic Carbonate Aminolysis. *Polym. Chem.* **2017**, *8* (41), 6349–6355.

(33)   Brutman, J. P.; Fortman, D. J.; De Hoe, G. X.; Dichtel, W. R.; Hillmyer, M. A. Mechanistic Study of Stress Relaxation in Urethane-Containing Polymer Networks. *J. Phys. Chem. B* **2019**, *123* (6), 1432–1441.

(34)   Elizalde, F.; Aguirresarobe, R. H.; Gonzalez, A.; Sardon, H. Dynamic Polyurethane Thermosets: Tuning Associative/Dissociative Behavior by Catalyst Selection. *Polym. Chem.* **2020**, 5386–5396.

(35)   Cash, J. J.; Kubo, T.; Dobbins, D. J.; Sumerlin, B. S. Maximizing the Symbiosis of Static and Dynamic Bonds in Self-Healing Boronic Ester Networks. *Polym. Chem.* **2018**, *9* (15), 2011–2020.

(36)   He, C.; Christensen, P. R.; Seguin, T. J.; Dailing, E. A.; Wood, B. M.; Walde, R. K.; Persson, K. A.; Russell, T. P.; Helms, B. A. Conformational Entropy as a Means to Control the Behavior of Poly(Diketoenamine) Vitrimers In and Out of Equilibrium. *Angew. Chemie - Int. Ed.* **2020**, *59* (2), 735–739.

(37)   Breuillac, A.; Kassalias, A.; Nicolaÿ, R. Polybutadiene Vitrimers Based on Dioxaborolane Chemistry and Dual Networks with Static and Dynamic Cross-Links. *Macromolecules* **2019**, *52* (18), 7102–7113.

(38)   Li, L.; Chen, X.; Jin, K.; Torkelson, J. M. Vitrimers Designed Both to Strongly Suppress Creep and to Recover Original Cross-Link Density after Reprocessing: Quantitative Theory and Experiments. *Macromolecules* **2018**, *51* (15), 5537–5546.

(39)   Hayashi, M.; Yano, R.; Takasu, A. Synthesis of Amorphous Low: T g Polyesters with Multiple COOH Side Groups and Their Utilization for Elastomeric Vitrimers Based on Post-Polymerization Cross-Linking. *Polym. Chem.* **2019**, *10* (16), 2047–2056.

(40)   Hayashi, M.; Yano, R. Fair Investigation of Cross-Link Density Effects on the Bond-Exchange Properties for Trans-Esterification-Based Vitrimers with Identical Concentrations of Reactive Groups. *Macromolecules* **2020**, *53* (1), 182–189.

(41)   Obadia, M. M.; Mudraboyina, B. P.; Serghei, A.; Montarnal, D.; Drockenmuller, E. Reprocessing and Recycling of Highly Cross-Linked Ion-Conducting Networks through Transalkylation Exchanges of C-N Bonds. *J. Am. Chem. Soc.* **2015**, *137* (18), 6078–6083.

(42)   Zhou, X.; Obadia, M. M.; Venna, S. R.; Roth, E. A.; Serghei, A.; Luebke, D. R.; Myers, C.; Chang, Z.; Enick, R.; Drockenmuller, E.; Nulwala, H. B. Highly Cross-Linked Polyether-Based 1,2,3-Triazolium Ion Conducting Membranes with Enhanced Gas Separation Properties. *Eur. Polym. J.* **2016**, *84*, 65–76.

(43)   Lopez, G.; Granado, L.; Coquil, G.; Lárez-Sosa, A.; Louvain, N.; Améduri, B. Perfluoropolyether (PFPE)-Based Vitrimers with Ionic Conductivity. *Macromolecules* **2019**, *52* (5), 2148–2155.

(44)   Tang, J.; Wan, L.; Zhou, Y.; Pan, H.; Huang, F. Strong and Efficient Self-Healing Adhesives Based on Dynamic Quaternization Cross-Links. *J. Mater. Chem. A* **2017**, *5* (40), 21169–21177.

(45)   Smet, M.; Metten, K.; Dehaen, W. Synthesis of New AB(2) Monomers for Polymerization to Hyperbranched Polymers by 1,3-Dipolar Cycloaddition. *Collect. Czechoslov. Chem. Commun.* **2004**, *69* (5), 1097–1108.

(46)   Ye, Y. S.; Huang, Y. J.; Chang, F. C.; Xue, Z. G.; Xie, X. L. Synthesis and Characterization of Thermally Cured Polytriazole Polymers Incorporating Main or Side Chain Benzoxazine Crosslinking Moieties. *Polym. Chem.* **2014**, *5* (8), 2863–2871.

(47)   Besset, C.; Bernard, J.; Fleury, E.; Pascault, J. P.; Cassagnau, P.; Drockenmuller, E.; Williams, R. J. J. Bio-Sourced Networks from Thermal Polyaddition of a Starch-Derived α-Azide-ω-Alkyne AB Monomer with an A2B2 Aliphatic Cross-Linker. *Macromolecules* **2010**, *43* (13), 5672–5678.

(48)   Wei, K.; Wang, L.; Zheng, S. Organic-Inorganic Copolymers with Double-Decker Silsesquioxane in the Main Chains by Polymerization via Click Chemistry. *J. Polym. Sci. Part A Polym. Chem.* **2013**, *51* (19), 4221–4232.

(49)   Bräse, S.; Gil, C.; Knepper, K.; Zimmermann, V. Organic Azides: An Exploding Diversity of a Unique Class of Compounds. *Angew. Chemie - Int. Ed.* **2005**, *44* (33), 5188–5240.

(50)   Fenouillot, F.; Rousseau, A.; Colomines, G.; Saint-Loup, R.; Pascault, J. P. Polymers from Renewable 1,4:3,6-Dianhydrohexitols (Isosorbide, Isomannide and Isoidide): A Review. *Prog. Polym. Sci.* **2010**, *35* (5), 578–622.

(51)   Obadia, M. M.; Drockenmuller, E. Poly(1,2,3-Triazolium)s: A New Class of Functional Polymer Electrolytes. *Chem. Commun.* **2016**, *52* (12), 2433–2450.

(52)   Chen, L.; Zhang, L.; Griffin, P. J.; Rowan, S. J. Impact of Dynamic Bond Concentration on the Viscoelastic and Mechanical Properties of Dynamic Poly(Alkylurea-Co-Urethane) Networks. *Macromol. Chem. Phys.* **2020**, *221* (1), 1–10.